Pergamon

PII: S0003-4878(00)00033-8

Ann. occup. Hyg., Vol. 45, No. 2, pp. 105–113, 2001

0003–4878/01/$20.00

A Model for Prediction of Fume Formation Rate in Gas Metal Arc Welding (GMAW), Globular and Spray Modes, DC Electrode Positive

JOHN H. DENNIS†, PETER J. HEWITT†, CHRISTOPHER A. J. REDDING†* and ANDREW D. WORKMAN‡

†Department of Environmental Science, University of Bradford, Bradford BD7 1DP, UK; ‡AWE plc, Aldermaston RG7 4PR, UK

Prediction of fume formation rate during metal arc welding and the composition of the fume are of interest to occupational hygienists concerned with risk assessment and to manufacturers of welding consumables. A model for GMAW (DC electrode positive) is described based on the welder determined process parameters (current, wire feed rate and wire composition), on the surface area of molten metal in the arc and on the partial vapour pressures of the component metals of the alloy wire. The model is applicable to globular and spray welding transfer modes but not to dip mode. Metal evaporation from a droplet is evaluated for short time increments and total evaporation obtained by summation over the life of the droplet. The contribution of fume derived from the weld pool and spatter (particles of metal ejected from the arc) is discussed, as are limitations of the model. Calculated droplet temperatures are similar to values determined by other workers. A degree of relationship between predicted and measured fume formation rates is demonstrated but the model does not at this stage provide a reliable predictive tool. © **2001 British Occupational Hygiene Society. Published by Elsevier Science Ltd. All rights reserved.**

Keywords: modelling; fume; metal arc welding; welding

INTRODUCTION

Concerns with the potential health effects of fume emissions during metal arc welding have prompted investigations of methods for reducing fume formation rate (FFR) and the concentration of hazardous metals in the evolved fume. Both the FFR and the fume composition may be influenced by a number of factors and changes may be effected by process modification (Hewitt, 1994; Dennis *et al*., 1997). Following previous investigations in our laboratories into mathematical models of fume composition, for example Gray (1980) and Hewitt and Hirst (1991), an investigation into theoretical prediction of FFR was undertaken. Prediction of FFR combined with prediction of fume composition from process parameters would be of use both to manufacturers of welding consumables and equipment and to occupational hygienists. It would facilitate risk assessment considerations to be carried out alongside weld quality and cost assessment at the process design and selection stages. Combined with a fume dispersion and inhalation model it would allow prediction of welder exposure to individual hazardous components of welding fume, including compounds of Fe, Cr, Ni and Mn.

Fume formed in GMAW is derived from three main sources

1. Molten droplets at the tip of the electrode and falling through the arc (in dip mode the wire tip melts but free droplets are not formed)
2. The weld pool
3. Spatter

Metal transfer modes in DC GMAW are dip, globular and spray. Generally dip occurs at low currents and spray at high currents with globular occurring between dip and spray modes. Shield gas composition affects this behaviour. Practical welding usually avoids the globular mode and fume formation rates

Received 16 July 1999; in final form 18 May 2000.
*Author to whom correspondence should be addressed. Tel.: +44-113-250-7279; fax: +44-274-234231

Nomenclature

A_d	drop surface area (m^2)
A_w	wire cross sectional area (m^2)
C_p	drop specific heat capacity ($J\ kg^{-1}\ K^{-1}$)
e	charge on an electron (C)
E_i	evaporation rate per unit area for element i ($kg\ s^{-1}\ m^{-2}$)
G	Universal gas constant ($J\ mol^{-1}\ K^{-1}$)
H_f	wire latent heat of fusion ($J\ kg^{-1}$)
H_L	wire tip volumetric heat content ($J\ m^{-3}$)
H_{vFe}	latent heat of vaporisation Fe ($J\ kg^{-1}$)
H_{vMn}	latent heat of vaporisation Mn ($J\ kg^{-1}$)
I	current (A)
j_w	wire current density ($A\ m^{-2}$)
k	Boltzman's constant ($J\ mol^{-1}\ K^{-1}$)
L	electrode extension (m)
L_a	arc length (m)
M_i	molecular weight element i ($kg\ mol^{-1}$)
o_d	drop density ($kg\ m^{-3}$)
o_w	wire density ($kg\ m^{-3}$)
P_i	pure vapour pressure element i ($N\ m^{-2}$)
Q_c	electron condensation heating (J)
Q_E	evaporation energy loss (J)
Q_R	resistive heating in droplet (J)
dQ_R/dt	rate of change of resistive heating ($J\ s^{-1}$)
R_d	droplet radius (m)
σ_d	droplet resistivity (Ω m)
t	time (s)
t_f	droplet falling time (s)
T_a	ambient temperature (K)
T_d	droplet temperature (K)
T_p	plasma (arc) temperature (K)
u_m	droplet maximum velocity ($m\ s^{-1}$)
u_w	wire velocity ($m\ s^{-1}$)
v_d	droplet volume (m^3)
V_a	anode potential (V)
V_c	condensation potential of electrons (V)
V_{wf}	droplet material work function potential (V)
ω	droplet transfer frequency (s^{-1})
x_i	mass fraction element i in wire ()
X_i	mole fraction element i in wire ()

for dip mode are usually lower than for spray mode. In dip mode the welding wire is fed at a rate greater than the melting rate, the wire shorts the arc leading to rapid heating of the wire and formation of a narrow neck which ruptures and the arc is re-established. This process occurs many times per second. Rupture of the narrow neck can result in production of micrometre-sized particles and so form fume. Overall temperatures are lower than for globular and spray welding modes and droplets are not normally formed. Work by Gray (1980) has indicated that the workpiece makes a minor contribution to fume formation. For GMAW Dennis and Mortazavi (1996) found 6–14% fume came from spatter. Gray (1980) measured 35% fume from spatter. In many cases the majority of fume in globular and spray welding modes is produced from droplets. The predictive model for FFR in GMAW considered here is limited to calculation of evaporation from droplets and is not directly applicable to dip mode. Fume may be formed by mechanisms other than evaporation, for example through bursting of bubbles of CO formed in droplets. Contributions to the fume from the weld pool, spatter and mechanisms in the arc other than evaporation are outside the scope of the present model.

METHODS AND MATERIALS

Fume was collected at the top of a conical fume hood of similar construction to that recommended by the American Welding Society (AWS, 1979). The chamber covered both the workpiece and the welding torch. An extraction pump system was used to remove fume from the fume hood to where it was collected on a Whatman GF/A glass fibre filter. The mass of fume was measured by weighing the filter before and after fume collection. Table 1 gives details on the welding wire and welding conditions. The welding power supply was a constant voltage Murex SMR 500 rectifier with TF2.0S wire feed unit and MXA503 air-cooled torch. Using a constant workpiece to contact tip distance (standoff) the arc length was varied, at each set voltage, by altering the feed rate of the consumable electrode until an arc length of 5 mm was established. Arc length was measured using a pinhole camera which projected an image of the arc onto a graduated screen. The screen was positioned so that the image was the same size as the arc. Current, voltage and wire feed rate were recorded using an ARCWATCH™ modular monitoring system for welding (Medcen Ltd). The associated monitoring software was used to calculate the mean and standard deviation from the mean for each of the parameters. It was also able to identify the peak levels in each parameter and then calculate the drop transfer frequency from the interval between the bottom of the peaks in either of the voltage or current signals. The wire electrode extension was assumed to be standoff less arc length although due to arc pressure the base of the arc may be below the surface of the workpiece.

THEORY

The modelling procedure involved calculations for the following five stages

1. Energy balance on wire and forming droplet to give initial droplet temperature, T_d(initial).
2. Initial evaporation rates for Fe and Mn calculated from T_d(initial) and wire composition.
3. Mass and energy balances on forming droplet over small time increments and summed over the formation period.
4. Falling time calculation for droplet based on literature values for average droplet velocity as a function of current.
5. Mass and energy balances on falling droplet over small time increments and summed over the falling period.

The time increment chosen for the forming droplet was 1/100th of the formation time and for the falling droplet 1/100th of the falling time. Computer spreadsheet software, such as Microsoft EXCEL, running on a 486 machine was more than adequate to perform the calculations using these time increments. Time increments should be short relative to rate of change of droplet composition and temperature but the shorter the time increment the longer the computing time and the more memory required. The resulting output from the spreadsheet gives droplet temperature, mass, composition and evaporation rate values for each time increment for both forming and falling stages.

An extract from the spreadsheet, adapted for this paper, is shown in Fig. 1.

The droplet mass increases with time at a rate determined by the wire feed velocity, cross-sectional area and density. The volume of the droplet is related to its mass by the density of the droplet.

$$v_d = \frac{u_w A_w o_w t}{o_d} \quad (1)$$

Droplet density is evaluated as a function of droplet temperature. A second order polynomial equation was fitted to data for density of liquid 304 stainless steel at different temperatures from Zacharia *et al*. (1991). This approximated the density of the Si–Mn alloy used for the model.

$$o_d = 7586 - 0.1546(T_d) - 0.0001411(T_d^2) \quad (2)$$

The droplet mass had to be corrected by subtracting evaporation losses. Assuming the droplet to be spheri-

Table 1. Welding wire and conditions

Wire electrode	Murex Bostrand BW1						
Typical wire composition	C	Mn	Si	S	P	Mo	Fe
(wt%)	0.08	1.2	0.8	0.02	0.02	0.25	97.65
(mol%)	0.37	1.21	1.58	0.03	0.04	0.14	96.63
Diameter	1.2×10^{-3} m						
Stand-off ($L+L_a$)	3.5×10^{-2} m						
Arc length (L_a)	5.0×10^{-3} m						
Welding polarity	DC electrode positive						
Shield gas	BOC Argoshield 5						
Shield gas composition	93%Ar, 5%CO_2, 2%O_2						
Flow rate	7.8×10^{-4} m^3 s^{-1} (47 l. min^{-1})						

DYMOD99 MODEL FOR EVAPORATION FROM A DROPLET (MFRU Bradford April 2000)									Calculations for data point 6 with smoothed u_w value				
DATA SET				**ENERGY+MASS BALANCE:FORMING DROPLET WITH 1/100 INCREMENT**									
x_{Fe}	0.976	wt.fraction		Time	Temp.	Fe mass	Mn mass	volume	Evaporation		Evap.	Resistance	
x_{Mn}	0.012	wt.fraction		N/(100ω)	T_d	Fe_d	Mn_d	v_d	t^*E_{Fe}	t^*E_{Mn}	loss	gain	DT_d
A_w	1.13E-06	m		1/s	K	kg	kg	m^3	kg	kg	W	W	K
L	3.00E-02	m		5.47E-05	2569	8.56E-08	1.05E-09	1.40E-11	4.86E-11	3.40E-11	8	14	4.70
L_a	5.00E-03	m		1.09E-04	2574	1.71E-07	2.07E-09	2.80E-11	7.95E-11	5.40E-11	14	22	5.57
p	ω	u_w	I	...	...	...	...	...	...	...	...	...	...
	1/s	m/s	A	...	...	...	...	...	...	...	...	...	...
1	33.4	0.093	175	5.47E-03	2545	8.50E-06	7.33E-08	1.38E-09	8.93E-10	4.65E-10	143	88	-24.17
2	80.9	0.105	188	5.53E-03	2545	8.50E-06	7.29E-08	1.38E-09	8.91E-10	4.62E-10	143	88	-24.63
3	130.7	0.127	212	EVAPORATION TOTAL FORMING					5.88E-08	3.28E-08			
4	122.4	0.155	240	**ENERGY AND MASS BALANCE:FALLING DROPLET WITH 1/100 INCREMENT**									
5	158.7	0.171	256	Falling time = $2L_a/u_m$		= t_f = 3.69E-03s							
6	**182.8**	**0.184**	**269**	Time	Temp.	Fe mass	Mn mass	volume	Evaporation		Evap.	Resistance	
7	172.4	0.207	294	Nt_f/100	T_d	Fe_d	Mn_d	v_d	t^*E_{Fe}	t^*E_{Mn}	loss	gain	DT_d
PHYSICAL PROPERTIES				1/s	K	kg	kg	m^3	kg	kg	W	W	K
o_w	7700	kg/m3		3.69E-05	2545	8.50E-06	7.29E-08	1.38E-09	6.01E-10	3.12E-10	143		-0.81
o_d	6258	kg/m3		7.38E-05	2544	8.50E-06	7.26E-08	1.38E-09	5.98E-10	3.09E-10	142		-1.61
σ_d	1.32E-06	ohm.m		...	...	...	...	...	...	...	...	...	...
C_p	753	J/kg.K		...	...	...	...	...	...	...	...	...	...
H_f	2.47E+05	J/kg		3.65E-03	2482	8.45E-06	5.04E-08	1.36E-09	3.92E-10	1.67E-10	89		-63.19
H_{vFe}	6.54E+06	J/kg		3.69E-03	2482	8.45E-06	5.03E-08	1.36E-09	3.91E-10	1.66E-10	89		-63.70
H_{vMn}	4.31E+06	J/kg		End	2481	8.45E-06	5.01E-08	1.36E-09					
T_p	10000K	T_a	293K	EVAPORATION TOTAL FALLING					4.81E-08	2.28E-08			
V_{wf}	4.18V	V_a	1.00V	EVAPORATION TOTAL FORMING + FALLING					1.07E-07	5.55E-08			

Fig. 1. Example of modelling spreadsheet.

cal approximated the surface area of the droplet, which is required for calculating the evaporation rate.

$$v_d = (4\pi/3)R_d^3 \tag{3}$$

$$A_d = 4\pi R_d^2 \tag{4}$$

Initial droplet temperature was calculated from an energy balance on the wire extension and molten droplet at its tip as shown in Fig. 2. Metal enters the system as solid wire at ambient temperature T_a and leaves as molten metal at T_d or as metal vapour. There is a gain in internal energy by the metal and this is derived mainly from resistance heating in the wire and electron condensation from the arc.

Internal energy gain = Net energy input

Resistance heating in the wire was calculated using a method described by Halmøy (1979). The heat content per unit volume at the end of the electrode extension as a result of resistance heating in the wire, H_L, was given by a second order polynomial curve fit to Halmøy's data

$$H_L = 1.69\times10^7 + 2.232\times10^{-7}\left(\frac{Lj_w^2}{u_w}\right) + 5.98\times10^{-23}\left(\frac{Lj_w^2}{u_w}\right)^2 \tag{5}$$

Electron condensation energy was given by

$$Q_c = V_c I t \text{ where} \tag{6}$$

$$V_c = V_{wf} + V_a + \left(\frac{3k}{2e}\right)(T_p - T_d) \tag{7}$$

Work function potential is composition and temperature dependent. According to Halmøy (1979) it falls by about 10^{-4}V K^{-1} as temperature rises. He quotes an average value of 4.4 V for Fe and a value of 3.8 V for Mn. The droplet is over 95% Fe so the value of 4.4 V was used with a correction assuming a droplet temperature of 2500 K. Anode fall potential was not measured. Richardson (1991) gives a typical value of 2.0 V for an argon shielded Tungsten Inert Gas (TIG) arc but work by Jönsson *et al.* (1995) indicates for GMAW a much lower value or even a negative value. Quinn *et al.* (1994) quote a value for V_c of 6.0 V for a GMAW model from which can be derived a value of 0.85 V for V_a assuming an arc temperature of 10 000 K and a droplet temperature of 2500 K. Metcalfe and Quigley (1975) conclude a value between 0 and 2 V for plasma arc welding and use a value of 1 V in their calculations. It seems reasonable to use a value of 1 V but this is an approximate figure. The third term on the right hand side of Eq. (7) results from the loss of kinetic energy of electrons in passing from the arc to the droplet. According to Richardson (1991) electron temperatures and ion/neutral temperatures are approximately equal at pressures above 0.1 bar. This condition applies to the

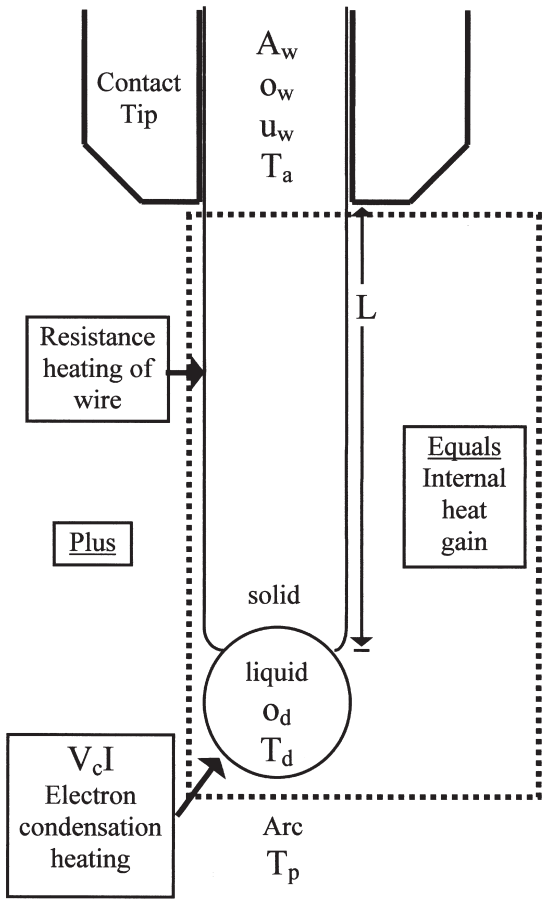

Fig. 2. Energy balance on wire electrode extension and molten droplet at its tip.

majority of welding arcs hence arc temperature (T_p) is used in place of electron temperature. Literature values for T_p in GMAW vary and depend on position in the arc. Lancaster (1987a) gives values for the arc column temperature of 6 000 K for an iron vapour arc and 10 000–15 000 K for a 200 A argon arc. Quigley and Webster (1972) give a value of 7500 K while Hermans and den Ouden (1996) and Zhu *et al*. (1997) use values of 10 000 K. Jönsson *et al*. (1994) give measured values from the centre of the arc axially outward with a value of 19 000 K at 0.2 mm and 9000 K at 5 mm. A mean value of 10 000 K was assumed for this model.

The energy balance can be written as

$$u_w A_w o_w \{C_p(T_d - T_a) + H_f\}t = H_L u_w A_w t + \left(V_{wf} + V_a + \left(\frac{3k}{2e}\right)(T_p - T_d)\right)It \quad (8)$$

Internal energy gain comprises sensible heat gain and latent heat of fusion in going from solid to molten metal. C_p is approximately constant between melting point and boiling point but is composition dependent. A value of 753 J kg^{-1} K^{-1} was used. H_f is also composition dependent. A value of 2.47×10^5 J kg^{-1} was used. Both these values are for steel and taken from Zacharia *et al*. (1991).

Equation (8) can be re-arranged to give

$$T_d(\text{initial}) = \left\{\frac{1}{1 + \left(\frac{3kI}{2eu_w A_w o_w C_p}\right)}\right\}\left\{T_a + \left(\frac{H_f}{C_p}\right) + \left(\frac{V_{wf} + V_a + (3k/2e)T_p}{u_w A_w o_w C_p}\right)I + \left(\frac{H_L}{o_w C_p}\right)\right\} \quad (9)$$

The rate of evaporation from molten droplets was estimated from the Langmuir equation derived from kinetic theory of gases for evaporation into a vacuum.

$$E_i = X_i P_i \left(\frac{M_i}{2\pi G T_d}\right)^{0.5} \quad (10)$$

Equation (10) gives the maximum possible evaporation rate per unit area for component i assuming no interaction between the components of the metal. Turkdogan *et al*. (1963) demonstrated that in the presence of oxygen, metal evaporation at atmospheric pressure can approach that predicted by the Langmuir equation. This is known as oxidation enhanced vaporisation whereby metal vapour reacts with oxygen near the surface of the metal forming an oxide, which condenses. The welding data given in this paper was obtained using a shield gas which contained 2% O_2 and 5% CO_2 which would have provided an oxidising atmosphere. CO_2 can dissociate to give CO and oxygen. Turkdogan's experiments on Fe were carried out at temperatures at or below 1873 K with the gas phase maintained at the same temperature as the metal. In the welding arc, droplet temperatures of over 3000 K have been measured and the surrounding plasma temperature is considerably higher. It is unlikely that oxidation enhanced vaporisation can occur under these conditions but using the Langmuir equation does provide a starting point which will over estimate evaporation. An alternative way to estimate evaporation rates would be by calculation of convective mass transfer from the surface of the droplet. Such calculations are beyond the scope of this paper. Only evaporation of Fe and Mn were considered. Other components of the wire were assumed to make up a constant proportion of the droplet. Vapour pressures of Fe and Mn were calculated using equations for pure vapour pressures as a function of temperature.

$$\text{Log}P_i = A + \left(\frac{B}{T_d}\right) + \left(\frac{C}{T_d^2}\right) \quad (11)$$

The coefficients for Mn and Fe are given in Table 2. The equations were taken from Gray (1980) and fit data from the National Physical Laboratory Data Bank. Correction for interactions were not made and the partial vapour pressures of Fe and Mn were given

Table 2. Vapour pressure equation coefficients

Element	A	B	C
Fe	10.41682	−15 724	−3 930 000
Mn	9.50342	−9246	−2 940 000

by $P_{pi} = P_i X_i$. Fe and Mn molecular weights are very similar so to simplify calculations mass fractions (x_i) were used in place of mole fractions. Following calculation of the initial droplet temperature and evaporation rate, mass and energy balances were performed on the forming droplet. Resistance heating in the droplet and evaporation losses were included. Calculations to estimate radiation and forced convection energy transfers with the arc indicated these were small compared to the evaporation loss but were comparable to the resistance heating at low currents. Estimated droplet power inputs and outputs at detachment are given in Table 3. Radiation and convection transfers were ignored but could be incorporated into a more complex model. Evaporation energy losses are

$$Q_E = A_d(E_{Fe}H_{vFe} + E_{Mn}H_{vMn})t \quad (12)$$

Resistance heating in the droplet was calculated by assuming it to be a cylinder of radius equal to that of the droplet at detachment ($R_d = R_{dmax}$) and length equal to twice the radius of a sphere of equal volume to the droplet. As the droplet grows the resistance heating changes so it is necessary to integrate the equation for the rate of change of resistance heating, dQ_R/dt.

$$\frac{dQ_R}{dt} = \sigma_d I^2\left(\frac{2R_d}{\pi(R_{dmax})^2}\right) \quad (13)$$

Using Eqs (1) and (3) and integrating Eq. (13) over the time period t_1 to t_2

$$Q_R = \sigma_d I^2\left(\frac{3}{2\pi}\right)\left(\frac{4\pi o_d}{3u_w A_w o_w}\right)^{1/3}\omega^{2/3}(t_2^{4/3} - t_1^{4/3}) \quad (14)$$

Using the above equations mass and energy balances were performed on the forming droplet over small time increments. From T_d(initial) droplet density was calculated and using Eq. (1) the volume of the droplet. Resistance heating and evaporation losses were also calculated and hence the mass of Fe and Mn lost from the droplet as well as the net energy gain. At the end of the first time increment new droplet temperature, mass and composition were calculated. The process was repeated for each time increment up to the time at which the droplet detached.

Table 3. Estimated droplet power inputs and outputs at detachment excluding wire resistance heating and electron condensation heating (in J s^{-1})

Data point	Q_E/t	Q_R/t	$Q_{convection}/t$	$Q_{radiation}/t$
1	−180	27	26	15
2	−94	39	19	10
3	−97	55	18	8
4	−202	66	20	8
5	−98	77	20	9
6	−134	88	19	8
7	−225	99	21	8

The arc plasma is a divergent conductor in which current induced forces produce a high plasma velocity. The arc plasma flowing past the droplet produces a drag force, which accelerates the detached droplet across the arc. Experimental measurement of droplet velocities by Needham *et al*. (1960) demonstrated a relationship between droplet maximum velocity and current. There was considerable scatter in droplet velocity at a given current but a linear regression line represented the trend. For GMAW welding with a mild steel, DC+ electrode and 0.005 m arc the line equation is

$$u_m = 0.019(I) - 2.4 \quad (15)$$

Assuming constant acceleration the average velocity is half the maximum velocity and so the falling time is

$$t_f = \frac{2L_a}{0.019(I) - 2.4} \quad (16)$$

The diameter of the electrode for mild steel was not given and this would affect droplet size and hence velocity at a given current. It is acknowledged that the estimation of droplet velocity requires further work if an accurate representation is to be achieved.

Given the droplet falling time, mass and energy balances on the falling droplet were calculated over increments of 1/100th of the falling time. There is no longer any gain in mass from the wire fed and energy gain from electron condensation and resistance heating was considered zero. The only mass and energy changes now are due to evaporation from the droplet (radiation and convection ignored as previously mentioned). Fe and Mn are lost as metal vapour and the required heat of vaporisation results in cooling of the droplet.

The droplet composition was re-calculated after each time increment for the forming and falling stages and the total loss of Fe and Mn from the droplet, over its lifetime evaluated. Multiplying by the droplet transfer rate (ω) then gave the metal evaporation rate (MER).

FFR was predicted from calculated metal evaporation rate (MER) based on work by Haidar *et al*. (1998). Haidar modelled condensation of metal vapour from arc onto workpiece. Assuming a thin boundary layer at the surface of the workpiece, within which all the metal vapour entering was condensed he

Table 4. Constants used in equations (see also Table 1)

C_p	753	J kg^{-1} K^{-1}	o_w	7700	kg m^{-3}
G	8.314	J mol^{-1} K^{-1}	σ_d	1.32×10^{-6}	Ω m
H_f	247 000	J kg^{-1}	T_a	293	K
H_{vFe}	6 535 000	J kg^{-1}	T_p	10 000	K
H_{vMn}	4 309 000	J kg^{-1}	V_a	1.00	V
$3k/(2e)$	1.29×10^{-4}	J K^{-1} C^{-1}	V_{wf}	4.18	V
M_{Fe}	0.05585	kg mol^{-1}			
M_{Mn}	0.05493	kg mol^{-1}			

predicted about 90% condensation with the remaining 10% forming fume. Analysis of fume from GMAW shows that it contains approximately 65% metal with the remaining 35% being mainly oxygen. Using these two factors the following relationship was obtained

$$\text{FFR(predicted)} = \left(\frac{1.0-0.9}{0.65}\right)\text{MER(calculated)} \tag{17}$$

The main equations from the theory section are repeated below for convenience of reference and constants used in calculations are given in Tables 1 and 4.

$$v_d = \frac{u_w A_w o_w t}{o_d} \tag{1a}$$

$$o_d = 7586-0.1546(T_d)-0.0001411(T_d^2) \tag{2a}$$

$$H_L = 1.69\times10^7 + 2.232\times10^{-7}\left(\frac{Lj_w^2}{u_w}\right) + 5.98\times10^{-23}\left(\frac{Lj_w^2}{u_w}\right) \tag{5a}$$

$$Q_c = V_c I t \text{ where} \tag{6a}$$

$$V_c = V_{wf} + V_a + \left(\frac{3k}{2e}\right)(T_p-T_d) \tag{7a}$$

$$T_d(\text{initial}) = \left\{\frac{1}{1+\left(\frac{3kI}{2eu_w A_w o_w C_p}\right)}\right\}\left\{T_a + \left(\frac{H_f}{C_p}\right) + \left(\frac{V_{wf}+V_a+(3k/2e)T_p}{u_w A_w o_w C_p}\right)I + \left(\frac{H_L}{o_w C_p}\right)\right\} \tag{9a}$$

$$E_i = X_i P_i\left(\frac{M_i}{2\pi G T_d}\right)^{0.5} \tag{10a}$$

$$\text{Log}P_i = A + \left(\frac{B}{T_d}\right) + \left(\frac{C}{T_d^2}\right) \tag{11a}$$

$$Q_E = A_d(E_{Fe}H_{vFe} + E_{Mn}H_{vMn})t \tag{12a}$$

$$Q_R = \sigma_d I^2\left(\frac{3}{2\pi}\right)\left(\frac{4\pi o_d}{3u_w A_w o_w}\right)^{1/3}\omega^{2/3}(t_2^{4/3}-t_1^{4/3}) \tag{14a}$$

$$t_f = \frac{2L_a}{0.019(I)-2.4} \tag{16a}$$

$$\text{FFR(predicted)} = \left(\frac{1.0-0.9}{0.65}\right)\text{MER(calculated)} \tag{17a}$$

RESULTS AND DISCUSSION

A set of welding experiments was performed as described in the Methods section. Table 5 gives the experimental data set used as input to the model. The results of the calculations to predict droplet temperature and FFR, over the current range used, are shown in Fig. 3 (T_d) and Fig. 4 (FFR). Figure 4 also includes additional experimental FFR results obtained under conditions close to those given in Tables 1 and 5. The calculations produced droplet temperatures for each time increment. Predicted temperatures for when the droplet starts to form, when it is about to detach and when it enters the weld pool are shown in Fig. 3. The predicted values are consistent with experimental determinations and other predictions of droplet temperature, some of which are given in Table 6. Lancaster (1987b) gives details of drop temperature variation

Table 5. Experimental data set

Data point	ω (s^{-1})	u_w (m s^{-1})	I (A)	FFR (kg s^{-1})
1	33.4	0.091	175	4.67×10^{-6}
2	80.9	0.108	188	
3	130.7	0.129	212	3.45×10^{-6}
4	122.4	0.148	240	
5	158.7	0.175	256	
6	182.8	0.185	269	4.68×10^{-6}
7	172.4	0.207	294	8.15×10^{-6}

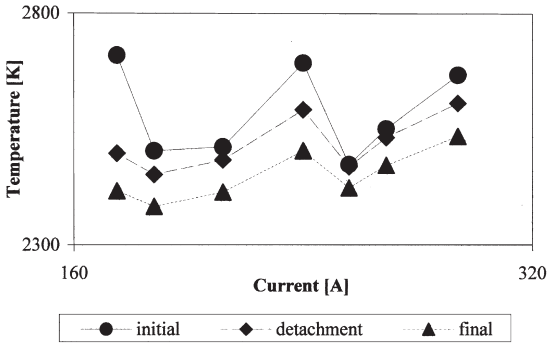

Fig. 3. Predicted droplet temperatures.

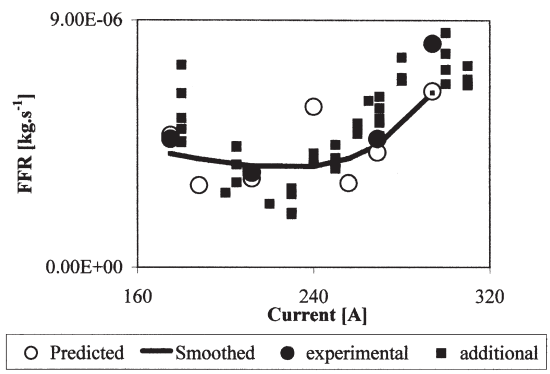

Fig. 4. Fume formation rate, experimental and predicted.

Table 6. Summary of droplet temperature measurements and predictions

Source	Temperature	Type
Model	2474–2710 K	Predicted mean
Lancaster (1987b)	2673 K	Thermocouple
Lancaster (1987b)	2273–2973 K	Calorimetric
Pollard and Milner (1971)	2673–2773 K	Predicted surface
Halmøy (1979)	2000 K	Predicted mean

with current for argon-shielded GMA using a 1.2 mm mild steel wire. The measurements were done pyrometrically by Villeminot (1966). There was a linear rise between 100 and 300 A from approximately 2600 to 3100 K. This is not followed by the predicted results. Very limited data were collected for GMAW in which current, wire velocity, droplet transfer frequency, arc length and fume formation rate were all measured. It is possible that the peak at 240 A in Fig. 3 (resulting in Fig. 4 peak) was probably due to erroneous input data measure. The three variable inputs to the model, for the data set in Table 5, are current, wire velocity and droplet transfer frequency. The model is fairly insensitive to droplet transfer frequency but is very dependent on the ratio of current to wire velocity (I/u_w). The ratio occurs in Eqs (5), (9) and (14). The change in this ratio with current is shown in Fig. 5. A smooth curve was fitted to the points and the ratios derived from this curve were then used to re-calculate FFR. The curve shown in Fig. 4 is fitted to the resulting FFR predictions. The original predicted values behave differently from the experimental values at 240 A but the predicted curve resulting from use of the smoothed I/u_w values is a much better fit to the experimental FFR values. More input data is required for a statistically meaningful comparison of the predicted and experimental FFR results.

The production of fume during metal arc welding involves a complex sequence of processes and there are many questions raised by the simplified model described here. The model relies on the Langmuir equation for evaporation into a vacuum and the significant limitations of this assumption have already been indicated in the Theory section.

Our earlier experimental studies have shown that shield gas composition can influence FFR. Removing all the oxygen from the shield gas and surrounding atmosphere dramatically reduces FFR. The proposed model does not address such effects but simply assumes that the oxygen and carbon dioxide (dissociated to CO and $^1/_2O_2$ in the arc) present provided sufficient oxygen for oxidation enhanced evaporation to approach that predicted by the Langmuir equation. The supply of oxygen from the shield gas, which contains 2% oxygen and 5% carbon dioxide, would be sufficient for oxidation of the metal vapour. It is assumed Fe initially forms FeO. FeO has a boiling point of 2700 K and decomposes at 3400 K; it is therefore unlikely to be present as a condensed phase in the boundary layer between the droplet surface and the arc plasma. Shield gas composition will also affect anode potential, V_a, which in turn will affect the electron condensation energy available.

Other limitations to the proposed model are recognised. We have assumed that 90% of the metal vapour re-condenses on the weld bead or weld pool relying on work by Haidar *et al.* (1998) but the welding conditions are likely to affect this figure. The model assumes spherical droplets of a constant size at any

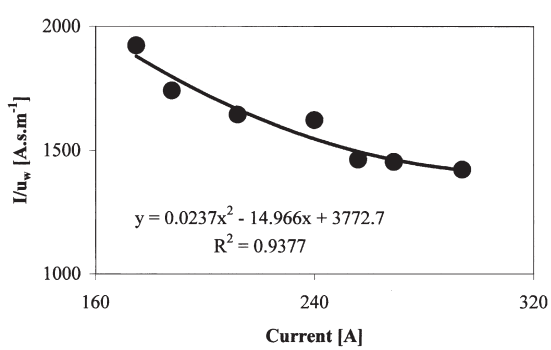

Fig. 5. Current to wire velocity ratio.

given current. Zhu *et al*. (1997) have shown there to be a distribution of droplet sizes at a particular current and the droplets are far from spherical for much of their existence. This would affect droplet falling times as well as temperature and evaporation. Contributions to the fume from the workpiece are not included. Such contributions have been demonstrated in our earlier studies to be small in comparison to the total quantity of fume produced. Contributions from spatter have also been disregarded.

To limit complexity this basic model relies heavily on empirical inputs. These include droplet transfer rates, arc length and droplet falling time. A more complex model could incorporate calculation of these quantities using a theoretical approach. Droplet transfer rates and shapes have been predicted by Haidar and Lowke (1996) from theoretical considerations. Halmøy (1979) has developed a method for calculating electrode extension using wire properties from which arc length can be derived given the standoff. Other possible improvements include incorporation of radiation and convection energy transfers, more accurate values for V_a and T_p and incorporation of the effects of shield gas composition.

The model has been applied to one mild steel consumable using direct current, electrode positive welding. The model is not sufficiently refined at this stage to enable recommendations to be made for changes to consumable composition, process parameters and shield gas composition which will minimise fume production. A degree of relationship between predicted and measured fume formation rates is demonstrated but the model is far from providing a reliable predictive tool.

Finally the model for GMAW is only applicable to globular and spray transfer modes the latter of which is commonly used for high deposition rate welding. The model described here has many limitations but it does provide a platform for future development.

Acknowledgements—This study was carried out as part of work supported by EPSRC Grant GR/K51754. Welding equipment and consumables were supplied by ESAB(UK). Experimental data was gathered with the assistance of Dr I.M. Richardson (Cranfield University) and Dr J. Norrish (previously of Cranfield University and now Professor at the University of Wollongong).

REFERENCES

AWS. Laboratory Methods for Measuring Fume Generation Rates and Total Fume Emissions of Welding and Allied Processes. Miami (FL): American Welding Society, 1979.

Dennis JH, Mortazavi SB. The mechanism of fume and spatter formation in MIG welding. Metal Fume Research Unit Occasional Technical Report 9608, University of Bradford, 1996.

Dennis JH, Mortazavi SB, French MJ, Hewitt PJ, Redding CAJ. The effect of welding parameters on ultra-violet light emissions, ozone and chromium VI formation in MIG welding. Annals of Occupational Hygiene 1997;38:95–104.

Gray CN. Fume formation in electric arc welding. Ph.D. thesis, University of Bradford, 1980.

Haidar J, Bosworth M, Brooks G, Deam R, Simpson S. Understanding Welding Fume: CRC Project 97.44. Co-operative Research Centre: Materials Welding and Joining Project Meeting Report, CSIRO Woodville Australia, 1998.

Haidar J, Lowke JJ. Predictions of metal droplet formation in arc welding. Journal of Physics D: Applied Physics 1996;29:2951–60.

Halmøy E. Wire melting rate, droplet temperature and effective anode melting potential. Arc Physics and Weld Pool Behaviour. Proceedings of International Conference. Abington: The Welding Institute; 1979. p. 49–57.

Hermans MJM, den Ouden G. Heat transfer in short circuiting GMAW. IIW-212-898-96, International Institute of Welding, 1996.

Hewitt PJ. Reducing fume emissions through process parameter selections. Occupational Hygiene 1994;1:35–45.

Hewitt PJ, Hirst AA. Development and validation of a model to predict the metallic composition of flux cored arc welding fumes. Annals of Occupational Hygiene 1991;35:223–32.

Jönsson PG, Szekely J, Choo RTC, Quinn TP. Mathematical models of transport phenomena associated with arc welding processes: a survey. Modelling Simulations in Material Science and Engineering 1994;2:995–1016.

Jönsson PG, Szekely J, Madigan RB, Quinn TP. Power characteristics in GMAW: experimental and numerical investigation. Welding Journal 1995;74:23s–102s.

Lancaster JF. Metallurgy of Welding, 4th edn. London: Allen and Unwin, 1987.

Lancaster JF. The physics of fusion welding part 2: mass transfer and heat flow. IEE Proceedings 1987;134(Pt. B):297–316.

Pollard B, Milner DR. Gas–metal reactions in CO_2 arc welding. Journal of the Iron and Steel institute 1971;April:291–300.

Metcalfe JC, Quigley MBC. Heat transfer in plasma-arc welding. Welding Journal 1975;54:99s–103s.

Needham JC, Cooksey CJ, Milner DR. Metal transfer in inert gas shielded arc welding. British Welding Journal 1960;2:101–14.

Quigley MBC, Webster JM. Metal transfer in arc welding. International conference on welding research related to power plant. Paper 39. UK: CEGB Marchwood; 1972.

Quinn TP, Madigan RB, Siewert TA. An electrode extension model for gas metal arc welding. Welding Journal 1994;73:241s–7s.

Richardson IM. Introduction to arc physics. Welding Technology M.Sc., Cranfield Institute of Technology, 1991.

Turkdogan ET, Grieveson P, Darken LS. Enhancement of diffusion-limited rates of vaporisation of metals. Journal of Physical Chemistry 1963;67:1647–54.

Villeminot P. Pyrometrie photographique appliquée au soudage. IIW-212-83-66, International Institute of Welding, 1966.

Zacharia T, David SA, Vitek JM. Effect of evaporation on weld pool development. Metallurgical Transactions B 1991;22:233–41.

Zhu P, Rados M, Simpson SW. Theoretical predictions of the start-up phase in GMA welding. Welding Journal 1997;76:269s–74s.